Clim. Past, 10, 733–744, 2014
www.clim-past.net/10/733/2014/
doi:10.5194/cp-10-733-2014

Climate of the Past
Open Access

On the low-frequency component of the ENSO–Indian monsoon relationship: a paired proxy perspective

M. Berkelhammer[1,2], A. Sinha[3], M. Mudelsee[4,5], H. Cheng[6], K. Yoshimura[7], and J. Biswas[8]

[1]University of Colorado, Boulder, CO, USA
[2]University of Illinois, Chicago, IL, USA
[3]California State University, Dominguez Hills, CA, USA
[4]Climate Risk Analysis, Hanover, Germany
[5]Alfred Wegener Institute, Bremerhaven, Germany
[6]Institute for Global Environmental Change, Xian Jiatong, China
[7]Atmospheric and Oceanic Research Institute, Tokyo, Japan
[8]National Cave Research and Protection Organization, Raipur, India

Correspondence to: M. Berkelhammer (berkelha@uic.edu)

Received: 1 May 2013 – Published in Clim. Past Discuss.: 11 June 2013
Revised: 9 January 2014 – Accepted: 17 January 2014 – Published: 11 April 2014

Abstract. There are a number of clear examples in the instrumental period where positive El Niño–Southern Oscillation (ENSO) events were coincident with a severely weakened Indian summer monsoon (ISM). ENSO's influence on ISM precipitation has therefore remained the centerpiece of various predictive schemes of ISM rainfall for over a century. The teleconnection between ISM precipitation and ENSO has undergone a protracted weakening since the late 1980s, suggesting the strength of ENSO's influence on ISM precipitation may vary on multidecadal timescales. The recent weakening has occurred despite the fact that the ENSO system has experienced variance levels during the latter part of the 20th century that are as high as any period in the past millennium. The recent change in the ENSO–ISM coupling has prompted questions as to whether this shift represents a natural mode of climate variability or a fundamental change in ENSO and/or ISM dynamics due to anthropogenic warming or aerosol impacts on the ISM. Here we place the 20th century ENSO–ISM relationship in a millennial context by assessing the phase relationship between the two systems across the time spectrum using a a series of high-resolution reconstructions of ENSO and the ISM from tree rings, speleothems and corals. The results from all the proxies suggest that in the high-frequency domain (5–15 yr), warm (cool) sea surface temperatures in the eastern tropical Pacific lead to a weakened (strengthened) monsoon. This finding is consistent with the observed relationship between the two systems during the instrumental period. However, in the multidecadal domain (30–90 yr) the phasing between the systems is reversed such that periods of strong monsoons were, in general, coincident with periods of enhanced ENSO variability. This result is counterintuitive to the expectation that enhanced ENSO variance favors an asymmetric increase in the frequency of El Niño events and therefore a weakened monsoon system. The finding implies that the prominent multidecadal variability that characterizes the last 1000 yr of the ISM is not likely attributable to multidecadal shifts in ENSO. If there is a continued trend towards enhanced ENSO variance in the coming decades, the results presented here do not suggest this will force a reduction in ISM precipitation.

1 Introduction

An improved understanding of the dynamical relationship between the El Niño–Southern Oscillation (ENSO) and the Indian summer monsoon (ISM) has value in constraining future projections of the monsoon system. The ENSO-related Indo-Pacific tropical sea surface temperature (SST) anomalies have been considered as the dominant externally driven forcing of monsoon variability (Webster et al., 1998; Kumar et al., 2006). The dynamical linkage between these two

systems principally results from the SST-induced east–west shifts in the Walker circulation and its interaction with the regional monsoon Hadley circulation (Webster et al., 1998; Krishnamurthy and Goswami, 2000; Ashok et al., 2004). For example, El Niño's impact on ISM rainfall is particularly strong when the locus of deep atmospheric convection shifts to the central Pacific (central El Niño) and the strongest descending lobe of the Walker cell is focused over the eastern equatorial Indian Ocean (Fasullo and Webster, 2002; Kumar et al., 1999; Kumar et al., 2006) – driving an anomalous monsoon Hadley circulation whose descending limb suppresses the convection-driven monsoon rainfall over the Indian subcontinent. The extreme manifestation of this coupling is exemplified (albeit, sporadically) by the co-occurrence of large El Niño events and devastating droughts in the Indian subcontinent such as during 1876–1878, 1918–1919, and 1982–1983 (Kumar et al., 2006).

In observational data, the strength of the ENSO–ISM relationship (characterized by linear correlations between any of the broad indices of ISM rainfall and SST anomalies in the tropical Pacific, respectively) has varied on inter-decadal to multidecadal timescales exhibiting high (low) inverse correlations at times when the ENSO variance shows high (low) amplitude modulation (Torrence and Webster, 1999; Krishnamurthy and Goswami, 2000). This has led to the suggestion that ENSO influences ISM rainfall through the same physical mechanism on both interannual and interdecadal timescales and that the waxing and waning of the coupling is related to frequency/amplitude modulation of ENSO events and changes in the tropical Pacific mean state (Torrence and Webster, 1999). In addition, decadal shifts in the North Pacific SSTs (i.e., the Pacific Decadal Oscillation) also produce an influence on the strength of ENSO teleconnections (Gershunov and Barnett, 1998). The recent breakdown in the relationship between the two systems (e.g., Kumar et al., 1999) has, however, occurred in the context of increased ENSO variance since the 1980s, with the late 20th century ENSO variability reaching a level as high as any other period during the last millennium (Li et al., 2011; Cobb et al., 2003, 2013). A range of hypotheses have been offered to explain the recent breakdown: global warming (Kumar et al., 1999), a southeastward shift of the subsiding limb of the Walker cell (Collins et al., 2010), changes in the ENSO spatial characteristics (Kumar et al., 2006), and the co-occurrence of ENSO and Indian Ocean Dipole (IOD) events (Ashok et al., 2004; Ummenhofer et al., 2011). In contrast, it has been argued that the relationship has largely remained intact and any fluctuations in its strength are merely a sampling artifact such that low-frequency changes in the correlation statistics between ENSO and the ISM time series occur much in the manner expected from purely stochastic processes (Gershunov et al., 2001) .

Understanding the nature of the ENSO–ISM relationship and specifically constraining the dynamics that have generated the recent change in the coupling between the systems is a problem ideally suited for general circulation models (GCMs) (e.g., Jourdain et al., 2013) where the response of the systems to various forcing mechanisms could be tested. However, systematic errors in simulating the mean state and variability of both ENSO and the ISM systems have hampered the ability to utilize this tool (Annamalai et al., 2007; Collins et al., 2010). Therefore, neither empirical observations, because of their brevity, nor model simulations are adequate in assessing the long-term nature of the influence that ENSO has on the ISM. As a consequence, there are significant limits on the predictability of the monsoon system across timescales. For example, if the recent increase in ENSO variance represents long-term trends towards a more active ENSO system, it would be important to predict whether this would in turn lead to a shift in the mean state of the monsoon. Proxy reconstructions of ENSO and ISM can therefore provide constraints on the nature of this coupling, particularly in the low-frequency domain under varying climate boundary conditions. Here we utilize a number of high-resolution, well-dated reconstructions of the two systems from tree rings, speleothems and corals to test whether multi-decadal shifts in ENSO variance have a consistent influence on the ISM system.

2 Methods

2.1 Monsoon reconstructions

A number of previous studies (e.g., Berkelhammer et al., 2010; Sinha et al., 2007, 2011) have demonstrated that ISM variability can be robustly reconstructed on a variety of timescales using the oxygen isotopic variability (δ^{18}O) of speleothems from central India. Here, we utilize a continuous 1400-year-long ISM reconstruction derived from a pair of overlapping speleothems from two sites: Dandak and Jhumar caves, located at ∼19° N; 82° E in the southern region of the core monsoon zone (CMZ) defined as ∼18–27° N and 69–88° E (Fig. 1). Details on the sampling methodologies and age models of these two records are described in previous studies (Berkelhammer et al., 2010; Sinha et al., 2011), and for the purpose of this study we have taken the two published records (NCDC), linearly interpolated them to an annual timescale and averaged the two (over the period of overlap) to produce a composite δ^{18}O record. We deem this compositing valid as the δ^{18}O profiles from Jhumar (2007–1075 AD) and Dandak (1562–625 AD) are well correlated over the period of overlap ($r = 0.62$, $n = 353$; 95 % [0.43; 0.74]), suggesting the independent age models are robust and the isotopic variability is not a function of the local cave environment (Fig. 1).

There is a significant (inverse) correlation between the speleothem δ^{18}O and CMZ JJAS precipitation (defined as the average of instrumental JJAS precipitation from 18 to 27° N and 69 to 88° E) time series during the instrumental

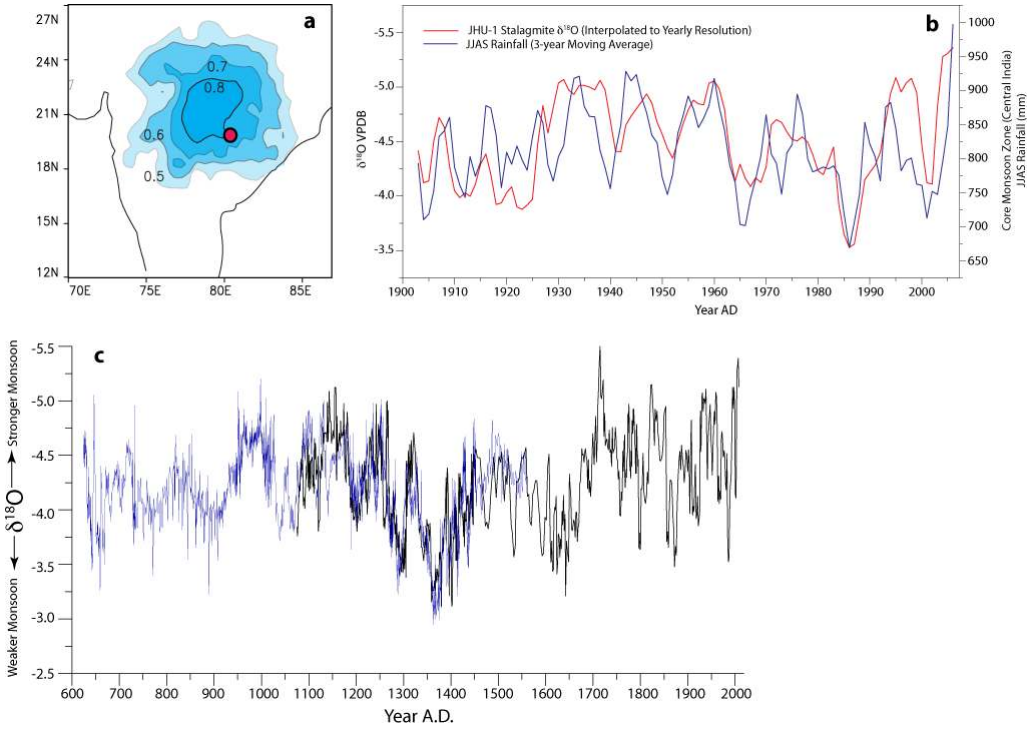

Fig. 1. **(a)** Correlation map between JJAS precipitation and regional precipitation across India. The result indicates the significance of this site as a broad indicator of CMZ monsoon precipitation. **(b)** The 20th century section of the speleothem δ^{18}O and JJAS rainfall. The observed precipitation amounts were treated with a 3 yr smooth to mimic mixing of waters in the karst. **(c)** The complete δ^{18}O time series from the JHU-1 (black) and Dandak (blue) records. Details of these records can be found in Sinha et al. (2011) and Berkelhammer et al. (2010).

period (1903–2006 AD, $n = 70$, $r = -0.46$ with 95 % CI [−0.59; −0.32]) (Fig. 1). Significance and confidence intervals for the correlation estimates were obtained using block bootstrap resampling (Mudelsee, 2010), which takes into account deviations from normal distributional shape and temporal autocorrelation. Further validation of the skill of this proxy comes from the observation that the record captures a number of known historical droughts such as those during 1876–1878, 1861–1863, and 1790–1796 AD (Sinha et al., 2007) and captures the series of protracted regional monsoon "megadroughts" in the late 14th century observed in tree ring records from SE Asia (Buckley et al., 2010; Sinha et al., 2007).

The robustness of the speleothems in capturing monsoon variability arises from the presence of a strong "amount effect" (Dansgaard, 1964) over south Asia, which has been documented in both modeling and observational studies (Dayem et al., 2010; Vuille et al., 2005; Pausata et al., 2011). In order to test the regional manifestation of the "amount effect", we utilize simulations with a nudged isotope-enabled GCM, IsoGSM (Yoshimura et al., 2008), which has been validated for parts of India in a previous study (Berkelhammer et al., 2012). The model shows that the region from where this proxy was generated experiences a strong inverse relationship between the δ^{18}O in the precipitation ($\delta^{18}O_p$) and the modeled area-weighted precipitation amount over the CMZ (Fig. 2). Similar correlation coefficients are also found for other broad ISM rainfall indices in the isotope simulations such as the homogeneous monsoon zone and the Indian monsoon index (IMI) (Wang and Fan, 1999; Wang et al., 2009), indicating the isotopic ratio in the precipitation at this site is a broad indicator of monsoon strength and not sensitive to domain boundaries or the choice of monsoon index.

The sensitivity of the isotopes in the precipitation, and consequently the speleothem proxy, to the overall strength of the Indian monsoon system arises because of its location at the near distal end of the landward portion of the low-level jet that is the primary conduit for moisture transport from the Arabian Sea onto the Indian subcontinent (Fig. 2). As a consequence, the isotopic ratio in the vapor and the precipitation at this site aggregate all upstream processes (e.g., rainout) that have influenced the Arabian Sea branch of the monsoon system as it crosses the continent (Fig. 2). For example, mean westerly flow is weaker with a large reduction in moisture flux during anomalous monsoon seasons associated with El Niño events (Fasullo and Webster, 2002). The low-level jet generates strong cyclonic vorticity in the boundary layer that aids in the initiation of convection over the entire CMZ region. The convective-related monsoon rainfall variability in the CMZ is significantly correlated ($r = 0.75$,

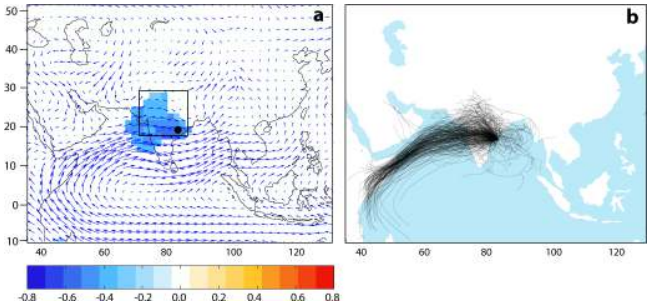

Fig. 2. (a) Correlation between JJAS $\delta^{18}O_p$ from nearest grid cell to the proxy and the precipitation rates in the surrounding grid cells using the IsoGSM model of Yoshimura et al. (2008). The analysis shows how upstream precipitation across India become aggregated in $\delta^{18}O_p$ at the proxy site. The vectors indicate the average surface wind fields during JJAS. **(b)** A composite of 2400 trajectories from 2002 to 2011 using the HYSPLIT model (Draxler and Rolph, 2003). Each trajectory was run for 90 h from the proxy site and initialized twice per day at 06:00 and 12:00 UTC at 1500 m a.g.l.

1901–2010 AD) to variations in the IMI region (Wang et al., 2009; Goswami, 1998) – broadly reflecting the large-scale rainfall variability in the region west of ∼80° E on intraseasonal (e.g., active and break periods) to inter-annual (e.g., ENSO) timescales. While the upstream processes that influence the isotopic ratio in the moisture are myriad, and therefore a direct transfer between rainfall amount and $\delta^{18}O_p$ is not likely stationary or linear, these collective monsoonal processes are the dominant control on the annually averaged $\delta^{18}O_p$ variability, explaining ∼25–30 % of the total variance of $\delta^{18}O$ in the speleothems.

An additional monsoon reconstruction is utilized by extracting all central Indian grid points from the Monsoon Asia Drought Atlas (MADA) (Cook et al., 2010). This is a gridded network of annually resolved JJA Palmer Drought Severity Index (PDSI) derived from over 300 tree ring width chronologies across Asia. The record extends from the present to 1300 AD, and while the network contains only a single chronology from central India, the grid points from India have strong verification statistics against instrumental PDSI, suggesting there is sufficient information in the network of the larger Asian monsoon system to capture variations in the ISM. For this study, an unweighted areal average JJA PDSI between 78–83° W and 14–21° N is taken to represent a broad indicator of monsoon strength (Fig. 3). The advantage of this proxy over the speleothem record described above is that it has an absolute annually averaged timescales, and therefore no consideration of age model uncertainty is needed. However, unlike the speleothem record, we presume some low-frequency variability of the monsoon system reconstructed from MADA is lost during the treatment of the tree ring data (Cook et al., 1995).

2.1.1 ENSO reconstructions

A number of attempts have been made to reconstruct continuous centennial to millennial length time series of ENSO variability by extracting inter-annually resolved climate signals from tree rings and corals (Emile-Geay et al., 2013; Li et al., 2011; Cobb et al., 2013; Mann et al., 2009). These reconstructions are generally well-calibrated and verified; though as a consequence of differences in the targeted index of ENSO to reconstruct, some significant differences can be found between the proxy records (Emile-Geay et al., 2013; Li et al., 2011). While the most accurate reconstructions of ENSO variability are presumably from proxies that are located within ENSO's center of action (i.e., the central tropical Pacific), such reconstructions are generally short and discontinuous. Proxy reconstructions from ENSO's teleconnected regions (such as the western USA) tend to be longer and continuous (e.g., Stahle et al., 1998; D'Arrigo et al., 2005) but rely on an assumption that the sign and strength of the teleconnection with ENSO has remained constant over time. Various ensembles of both direct and distal proxy reconstructions of ENSO show similar behavior at decadal scales, but the amplitude of multidecadal to centennial variability diverges between reconstructions as a result of inherent aspects of the proxy such as hysteresis effects, common in speleothems due to mixing in the karst, that favor low-frequency power or the "segment length curse" in tree ring proxies (Cook et al., 1995) that favors high-frequency power.

We utilize a remote ENSO-teleconnection-based tree ring proxy (Li et al., 2011), two continuous sections (∼1350–1450 and ∼1630–1700) of a coral-based ENSO reconstruction (Cobb et al., 2003) and a composite multi-proxy ENSO reconstruction that utilizes tree rings, corals, sediments and tropical ice cores (Emile-Geay et al., 2013). The former is a millennial-length, continuous reconstruction of the canonical (eastern Pacific) ENSO amplitude derived from the first principal component of the gridded North American Drought Atlas (NADA) – a large data set of tree-ring-based drought reconstructions (Cook et al., 2004) (Fig. 3). Li et al. (2011) derive ENSO variance by applying a bi-weight 21 yr running variance to the first principal component (PC-1) of NADA. The ENSO variance generated from the tree ring network is significantly correlated to various modern indices of ENSO and arises because of the dominant influence ENSO has on moisture availability (and consequently tree growth) in water-limited regions in western North America. While there is an important distinction between ENSO variance (the spread of the amplitude over a time window) and ENSO amplitude, variance tends to be a good proxy for El Niño strength because there is an asymmetrical quality to the ENSO system such that changes in variance tend to be driven by increases in the frequency of El Niño events (Anderson et al., 2013; Larkin and Harrison, 2002). The NADA ENSO record has excellent skill during the calibration period

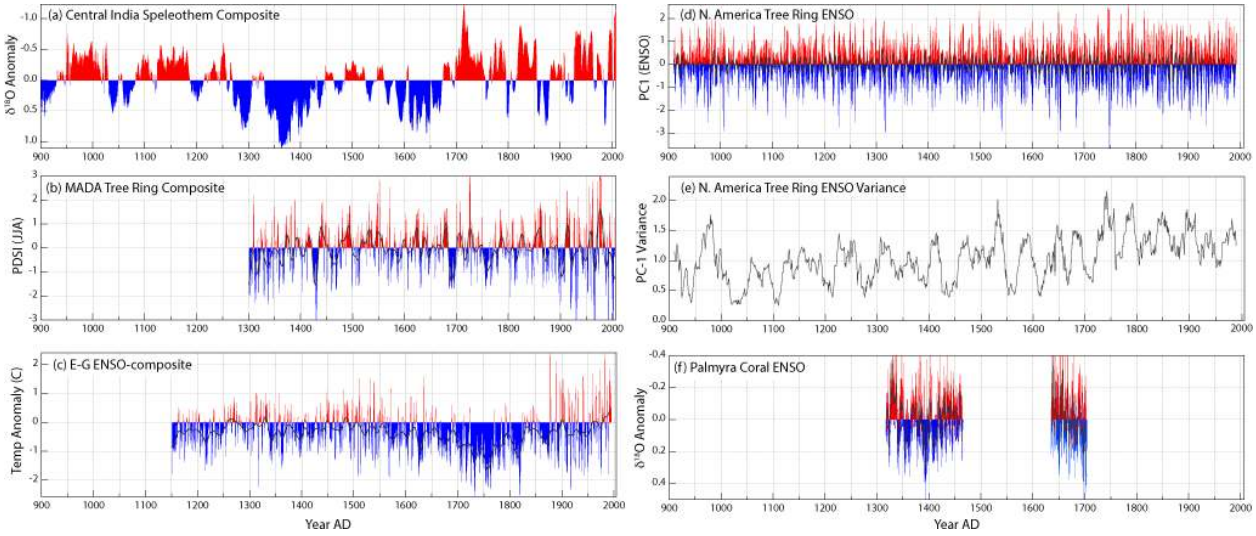

Fig. 3. **(a)** Annually interpolated speleothem monsoon reconstruction from Fig. 1 shown as isotopic (δ^{18}O) anomalies relative to the mean of the time series. *Y* axis is reversed so that dry periods point down. **(b)** The central Indian monsoon reconstruction based on the average of all grid points in central India from the MADA database (Cook et al., 2010). A Lanczos filter is applied to the data to accentuate variability in the 5–15 yr window. **(c)** Niño3.4 SST anomalies from the multi-proxy composite of Emile-Geay et al. (2013). The reconstruction uses the ERSSTv3 instrumental data to train the proxies. **(d)** The first principal component of the NADA network from Li et al. (2011), which largely reflects SSTs in the eastern tropical Pacific. A similar band-pass filter is applied to the data as in **(b)**. **(e)** The bi-weight variance of the PC-1 of the NADA ENSO reconstruction (Li et al., 2011). **(f)** Two long continuous sections of the Palmyra coral δ^{18}O time series from Cobb et al. (2003). As in **(a)**, the *y* axs is reversed so that warm SSTs are up.

and agrees with shorter-term proxy reconstructions of ENSO including those derived from discontinuous coral sequences from the tropical Pacific. This record is currently the longest interannual ENSO reconstruction spanning the last millennium. We utilize both the PC-1 (interannual ENSO amplitude) and the derived ENSO variance in estimations of the relationship between ENSO and the ISM.

We also utilize two multi-decadal coral δ^{18}O sequences from Palmyra Atoll in the central tropical Pacific to validate our findings using an alternative to the remote reconstruction (Fig. 3). Because of the brevity of the coral records, these data are not used to investigate low-frequency aspects of the ENSO–ISM coupling but rather to provide an additional independent and Pacific-based proxy. Lastly, the composite Niño3.4 reconstruction of Emile-Geay et al. (2013) is used as an additional validation of the results. This reconstruction composites multiple high-resolution tropical proxies to target variability in Niño3.4 SSTs. As discussed in Emile-Geay et al. (2013), the choice of instrumental SST data set to train the proxy influences the reconstructed centennial-scale variability, but the reconstruction is not sensitive to this choice at interannual to multidecadal timescales. Hereafter, we discuss the ENSO reconstruction using ERSSTv3 for validation though the results discussed do not vary markedly between data sets.

2.1.2 Model results

While the paper is intended to to deal primarily with proxy results, analysis of the ENSO–ISM coupling is also explored in two 1000 yr control simulations using the Goddard Institute for Space Studies (GISS) and Max Planck Institute (MPI) models from the CMIP5 database (Taylor et al., 2012). These two simulations have notably different skill in their ability to capture ENSO variability with the former (GISS) having a notably weaker representation (e.g., Zhang and Jin, 2012). However, testing the coupling of ENSO and the ISM is distinct from assessing the representation of ENSO or ISM independently. For example, a weak representation of ENSO in a given GCM may not imply the model does not capture the teleconnection that couples ENSO and the ISM. The analyses presented are not intended to be exhaustive but provide some insight into a methodology to study the nature of the coupling between ENSO and the ISM in state-of-the-art general circulation models. For both control simulations, the ISM is defined as the sum of precipitation amount from June to September between 78–83° W and 14–21° N, and ENSO (Niño3.4) is defined as the annually averaged SSTs for −170 to −120° W and −5 to 5° N. No additional processing was applied to the data extracted from the model simulations.

2.1.3 Phase estimation

In order to assess the ENSO–ISM teleconnection, we determined the coherence and phase angle between the two systems using combinations of the proxies listed above (e.g., coral ENSO vs. speleothem ISM, tree ring ENSO vs. tree ring ISM, speleothem ISM vs. composite ENSO). The advantage of a spectral approach, as opposed to correlation analysis, is it allows for a delineation of the relationship between these systems at different timescales. This is critical because by combining proxies, each favoring different parts of the spectrum (tree rings and corals favoring the high frequency and speleothems favoring the low frequency), a simple correlation between the time series yields ambiguous results regarding the nature of the ENSO–ISM teleconnection. The approach utilized here follows that described by Torrence and Webster (1999) to characterize the ENSO–ISM coupling but extends the analysis into lower frequency aspects of the relationship using the longer time series afforded from the proxy records. The phase angle between the overlapping periods of the aforementioned ENSO and ISM reconstructions is done using cross-spectral analysis with the multi-taper coherence method (Chave et al., 1987). The approach is based closely on the cross-spectral analysis technique described by Huybers (2004) where coherence is assessed at progressive windows spanning the time spectrum, and the phase angle is calculated by finding the lag that maximizes the correlation between the time series in each spectral window. For tree ring and coral proxies, the uncertainty in the phase angle is calculated using a Monte Carlo approach where the phasing of iterations of time series with similar spectral properties provides confidence bounds. These time series are assumed to have no age uncertainty. Uncertainty in the phase angle between the speleothem time series further considers the influence that age model uncertainty has in the phase angle estimation.

We focus the discussion hereafter on two windows of the time spectrum: a *high-frequency* band that includes all power in the 5–15 yr window and a *low-frequency* band encompassing power in the 30–90 yr window. The high-frequency band is intended to shed light on the long-term stability of the known dynamical connection between the ISM and ENSO during the instrumental period (Kumar et al., 1999). The high-frequency band should assess variations at the interannual timescale; however, as a consequence of multi-year mixing times for water in the karst, the speleothem monsoon proxy likely integrates variability across ∼3–8 yr. Therefore, we deem the 5–15 yr band as the highest frequency window in which confidence in the proxy can be asserted. The low-frequency window was chosen as a response to earlier work based on one of the speleothems in the composite, which showed the presence of strong multidecadal power of the ISM (Berkelhammer et al., 2010). The source of this multidecadal variability remains unknown as its period is too long to be studied using instrumental observations alone. The phase analysis presented here is intended, in part, to assess the role ENSO may play in pacing the dominant multidecadal power of the ISM.

To evaluate whether the differences in the phase angle between ENSO and the ISM in the low-frequency (30–90 yr) and high-frequency (5–15 yr) bands are significant against the age model uncertainties, we performed a numerical simulation where the timescales of two sinusoidal signals (frequencies f1 and f2 with predefined phase differences of d_{phi}) were perturbed with a Gaussian random number generator. We then estimated the phase difference for the jittered series, $d_{\mathrm{phi\_sim}}$, using a periodogram. The standard deviation of $d_{\mathrm{phi\_sim}}$ for the low-frequency bound f1 = 1/(30–90 yr) and the high-frequency bound f2 = 1/(5–15 yr) was calculated from 10 000 simulations.

The results are presented as phase wheels (Figs. 4 and 6) where the direction of the arrow relative to 0 ° (due right) represents the phase angle between the time series. The length of the arrows indicates the strength of the coherence, and only arrows where the phase angle is significant at the 90 % confidence interval is shown. The phase wheels can be interpreted as follows: a large number of arrows clustering near an angle suggests a strong likelihood that the two time series exhibit coherence at that spectral window. If only a few arrows are present near an angle, there is statistically significant coherence in this band, but we have less confidence that there is a persistent phase relationship in that window. All arrows that are green capture the phase angle for all bands in the high-frequency window (5–15 yr), whereas all arrows that are purple show the phase angle for each band in the low-frequency window (30–90 yr). Finally, before any phase analysis was conducted, the speleothem and coral proxies were inverted such that positive values capture strong ISM periods and warm ENSO conditions, respectively. As such, the "expected" relationship between ENSO and ISM time series is 180° (i.e., strong ENSO events being concurrent with diminished ISM precipitation).

3 Results

The cross-spectra and phase coherence between the speleothem ISM reconstruction and NADA PC-1 amplitude time series suggest that, in the high-frequency domain (5–15 yr), periods of positive ENSO amplitude were associated with reduced ISM rainfall (Fig. 4a). A qualitatively similar result emerges when the cross-spectra between the speleothem ISM and ENSO composite (EG) are calculated (Fig. 4b). However, there were notably fewer spectral bands where the coherence was significant using this ENSO reconstruction. A similar phase relationship (∼180°) emerges when the cross-spectra between the speleothem ISM and coral ENSO reconstruction from Cobb et al. (2003) are calculated (Fig. 4c). The consistency between proxies indicates

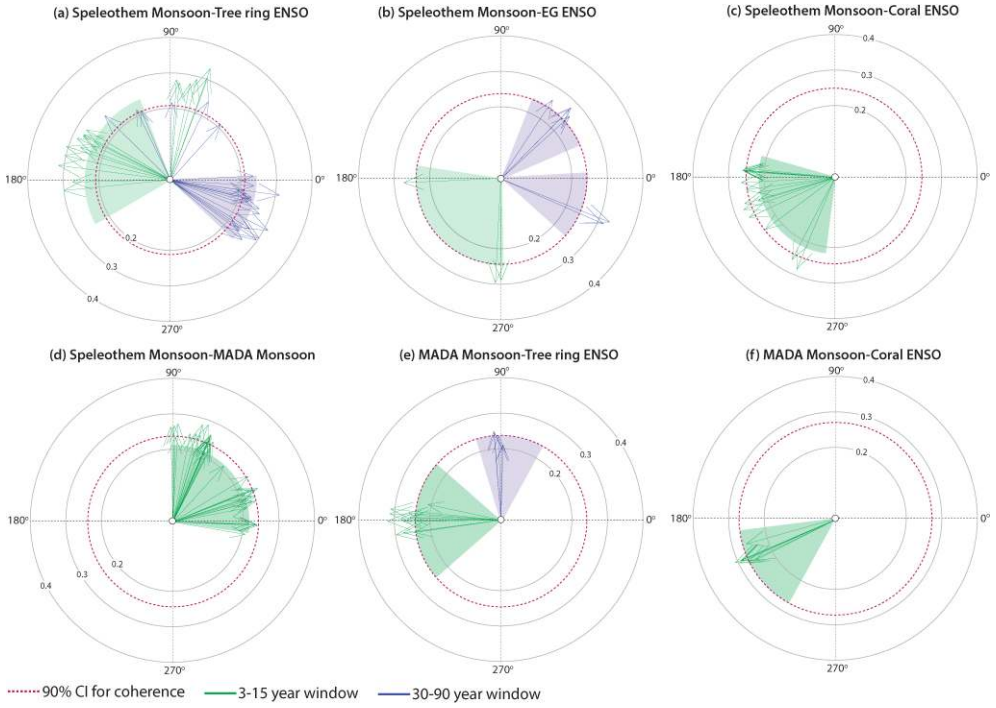

Fig. 4. Results from cross-spectral analysis between all proxy time series shown in Fig. 3. Arrows to the right indicate time series that are in phase with one another, while arrows to the left indicate time series that are anti-phased. Only arrows are shown when coherence between the time series is significant at the 90 % confidence interval. The length of the arrow indicates the strength of the coherence, and the concentric circles indicate increasing (labeled) levels of coherence. The shaded wedges indicate estimates of uncertainty, which accounts both for age model uncertainties and those that arise from noise in the time series. All green arrows and wedges are for phasing in the high-frequency (5–15 yr) window, and purple arrows and wedges are for phasing in the low-frequency (30–90 yr) windows. Lastly, the speleothem and coral time series were inverted such that for all analysis arrows to the left (right) indicate strong (weak) monsoon associated with weak ENSO. **(a)** Speleothem ISM (Sinha et al., 2011) against tree ring ENSO (Li et al., 2011), **(b)** speleothem ISM (Sinha et al., 2011) against composite ENSO (Emile-Geay et al., 2013), **(c)** speleothem ISM (Sinha et al., 2011) against coral ENSO (Cobb et al., 2003), **(d)** speleothem ISM (Sinha et al., 2011) against MADA ISM (Cook et al., 2010), **(e)** MADA ISM (Cook et al., 2010) against tree ring ENSO (Li et al., 2011), and **(f)** MADA ISM (Cook et al., 2010) against coral ENSO (Cobb et al., 2003).

that the phase angles are relatively insensitive to the choice of ENSO proxy, though the degree of significance does vary.

We find no statistically significant phase relationship between ENSO amplitude from NADA and the speleothem ISM reconstruction in the low-frequency (30–90 yr) domain. However, if the cross-spectral analysis is done using ENSO variance from Li et al. (2011), a coherent near-in-phase ($\sim$180°) relationship emerges (Fig. 4a). This result shows that multidecadal periods of enhanced ENSO variance were associated with generally stronger monsoons. The strength of the coherence appears to be particularly strong between 900 and 1500 AD though continues, albeit intermittently, after the 15th century (not shown). For example, some of the wettest intervals of the ISM occur after the 17th century coinciding with a multi-centennial period of the highest ENSO variance in the NADA PC-1 reconstruction. Results from the 10 000-iteration Monte Carlo simulation illustrate that even with conservative estimates of age model uncertainty, the difference in the phase angle between ENSO and the ISM time series in the high- and low-frequency windows is significant (Fig. 4a). We estimate uncertainty in the calculated phase angle could theoretically be as much as 52° while the phase angle difference we calculate is between 90 and 150°, showing this result is not an artifact of age model uncertainty.

As an additional test of the ENSO–ISM coupling, we also consider the phase relationship between ENSO reconstructions and the MADA-derived monsoon time series. In Fig. 4d, the cross-spectra between the two monsoon time series (speleothem and tree ring) are shown. The result shows the two proxies are nearly in phase with one another. While the phasing is not exactly 0°, as expected if the two proxies are responding to the same forcing, they generally are in phase within 1–3 yr (i.e., $\leq 90°$ of 5–15 yr). There is no statistically significant coherence between the two time series in the low-frequency domain, which is apparent in that the MADA time series misses a number of the significant sustained monsoon droughts observable in the speleothem record (Sinha et al., 2011). The MADA time series shows an anti-phased relationship with the NADA ENSO amplitude, further confirming the robustness of the finding that

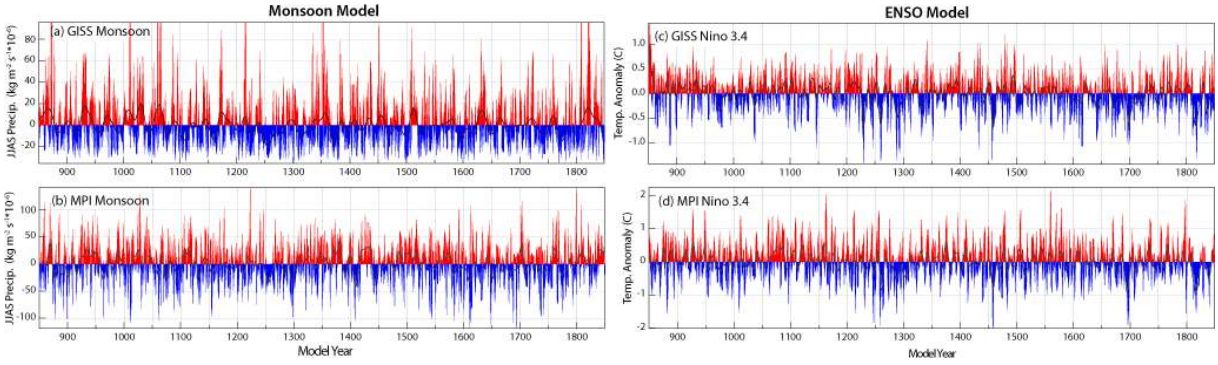

Fig. 5. Time series of the monsoon **(a, b)** and Niño3.4 **(c, d)** from the GISS **(a, c)** and MPI **(b, d)** models. The ISM precipitation is the sum of JJAS precipitation over India, and the ENSO time series is the annually averaged SSTs over the Niño 3.4 region. These 1000 yr monthly resolved data were taken from the CMIP5 database (Taylor et al., 2012). No additional processing such as normalization was applied to the data.

positive ENSO amplitude is associated with a weakened ISM (Fig. 4e). There is some indication of a 90° phase angle in the low-frequency window, but the coherence is of low significance. Finally, we test the coherence between ENSO and the ISM using the coral ENSO and MADA ISM proxies (Fig. 4f). The results here provide further evidence of coherent coupling between ENSO and the ISM in the high frequency.

To test the ENSO–ISM coupling in the model simulations, we calculate the coherence and phase angle between the model-derived ENSO and ISM time series (Fig. 5). The cross-spectral analysis using results from the GISS model shows that, in the high-frequency domain, positive (negative) ENSO amplitude leads to a weakened (strengthened) ISM with a very high degree of confidence (Fig. 6a). In the low-frequency domain, we also find some indication of a reversal of this phasing, similar to what was observed with the proxies (Fig. 4a). However, we acknowledge that the statistical significance of the phasing in the low frequency is weak (judging by the small number of arrows). The MPI model shows the same relationship as the GISS simulation in the high-frequency domain (inverse relationship) (Fig. 6b). However, contrary to GISS, the MPI simulation suggests a similar phase relationship between ENSO and the ISM in both the high- and low-frequency domains.

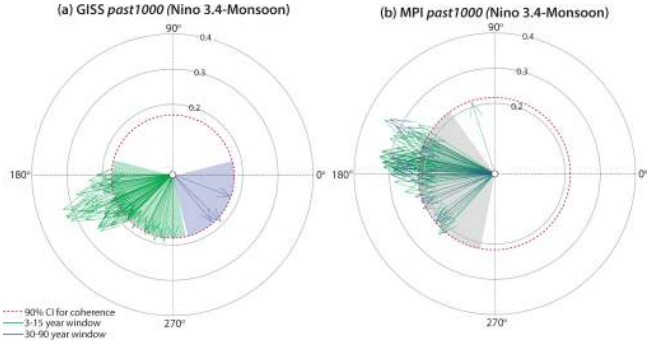

Fig. 6. Phase relationships between ENSO and the ISM for the two modeled time series in Fig. 5. Phase wheels can be interpreted identically to those shown in Fig. 4.

4 Discussion

An important finding that emerges from this study is that across a number of proxies, there is a persistent high-frequency coupling between the ISM and ENSO. The dynamics of this coupling (weak monsoon during positive ENSO events) has been discussed extensively with respect to instrumental data (e.g., Kumar et al., 2006). The proxy data show there has been a consistent influence of ENSO on the ISM over the last millennium. The nature of this coupling is also captured in the two model simulations analyzed here.

An important question that we can now assess with the proxy data is whether the persistent high-frequency ENSO–ISM coupling can explain the presence of strong multidecadal power in the ISM. Our a priori expectation was that because enhanced ENSO variance is driven by more frequent El Niño events, multidecadal periods of increased (decreased) ENSO variance would drive sustained periods of weakened (strengthened) ISM rainfall. Therefore, changes in the frequency of large or persistent El Niño events would produce low-frequency variability in ISM rainfall. The results presented in Fig. 4a imply, counterintuitive to our expectation, that a more active ENSO state occurs simultaneously with an increase in ISM rainfall. While we acknowledge the challenges and uncertainty in deriving low-frequency ENSO variance from NADA, a few pointed examples of periods of enhanced ENSO variance associated with a weakened ISM provide confidence in this finding. For example, the major ISM droughts of the late 14th century occur in the context of reduced ENSO variance based independently on the coral-based ENSO proxy of Cobb et al. (2003).

A number of mechanisms could explain the fact that periods of enhanced ENSO variance occur simultaneously with a strengthened ISM. One possible explanation is that changes in ENSO variance are being driven by an increase in La Niña events. This is somewhat contradictory to the assumed driver of changes in ENSO variance (Anderson et al., 2013), but if this were the case, periods of high variance would be associated with more La Niña events and consequently a stronger ISM. However, an analysis of the reconstructed ENSO distribution during periods of high variance does not indicate an asymmetry that favors La Niña (Fig. 7). An alternative explanation is that, in the low-frequency domain, the two systems are phase-locked through a common forcing mechanism, which leads to both an increase (decrease) in ENSO variance and a strengthened (weakened) ISM.

One mechanism to explain the presence of shared multidecadal power between these systems is through periodic variability in the North Atlantic SSTs. It is well-documented that North Atlantic SSTs are characterized by power with 50–90 yr periodicity (Enfield et al., 2001) and have an impact on both ENSO variance and ISM rainfall. Goswami et al. (2006) show that much of the multidecadal power of ISM rainfall during the instrumental period can be linked to shifts in North Atlantic SSTs. The authors argue that warming in the North Atlantic influences tropospheric temperatures over Eurasia and consequently the meridional temperature gradient over India. This change in the temperature gradient, in turn, leads to an increase in ISM rainfall. A similar finding has been shown on millennial timescales where warmer conditions in the North Atlantic are associated with a stronger monsoon (Gupta et al., 2003). A number of studies have also looked at the impact that changes in the North Atlantic SST fields have on ENSO variance. Timmermann et al. (2005) show that cooling of the North Atlantic leads to a deepening of the tropical Pacific thermocline, which stabilizes the ENSO system (i.e., reduces variance). While their analysis focused on millennial-scale events, the oceanic teleconnection mechanism they describe also operates in model simulations on multidecadal timescales. Therefore, positive (negative) SSTs in the North Atlantic would lead to both an increase (decrease) in ISM rainfall and ENSO variance. However, it must also be noted that the link between ENSO variance and North Atlantic SSTs proposed by Timmermann et al. (2005) is contrary to the findings of Dong et al. (2006), who describe the presence of an atmospheric bridge where cooling in the North Atlantic reduces easterly flow in the tropical Pacific leading to a shallower thermocline and *enhanced* ENSO variance. The difference between the findings of these studies is likely embedded in the fact that the former (i.e., Timmermann et al., 2005) focused on an oceanic teleconnection while the latter (i.e., Dong et al., 2006) focused on an atmospheric bridge. Because we are interested here primarily in the low-frequency nature of the ENSO–ISM coupling, it is appropriate to consider the oceanic mechanism as it would have a characteristic tendency for lower frequency power.

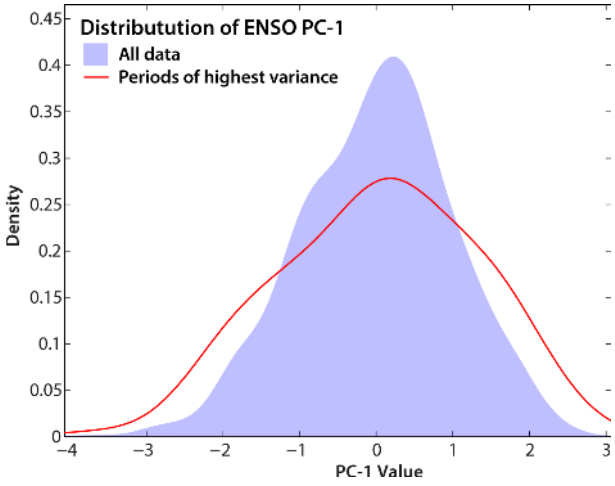

Fig. 7. Distribution of the annual PC-1 scores from Li et al. (2011) using all data (blue shading) and during windows of increased variance ($\geq$ 1.5, Fig. 3d). The distribution is wider during periods of increased variance but does not have a tail favoring La Niña.

An additional candidate to explain the low-frequency coupling of ISM and ENSO is through decadal variability in North Pacific, often characterized by the Pacific Decadal Oscillation (PDO) SST pattern (Mantua and Hare, 2002). The PDO has a warm and cold phase with a teleconnection pattern in the Northern Hemisphere that is similar to corresponding warm and cold phases of ENSO (Gershunov and Barnett, 1998). The PDO has a known influence on the ISM, such that the warm phase of the PDO is associated with a weakened ISM, as a consequence of a similar dynamical mechanism associated with a weakened ISM during warm ENSO events (Krishnan and Sugi, 2003). The PDO can mitigate or exacerbate the strength of ENSO teleconnections such that warm (cold) ENSO events coincident with warm (cold) phases of the PDO have enhanced teleconnection patterns, whereas warm (cold) ENSO events during cold (warm) PDO periods have a diminished influence on the Northern Hemisphere ENSO teleconnections (Gershunov and Barnett, 1998). Therefore, if there were anti-phased behavior between the PDO and ENSO, it could result in a strengthened ISM coincident with positive ENSO events.

Lastly, a number of recent studies such as that of Tierney et al. (2013) argue for a dominant role of dynamics internal to the Indian Ocean (IO) in producing multidecadal hydroclimate variability across the IO basin. IO dynamics are a critical source of variance in the monsoon (Ashok et al., 2004) and likely an important determinant of low-frequency monsoon behavior (Sinha et al., 2011). If the multidecadal power in the ISM is paced by internal dynamics in the IO, the positive phasing between ENSO and the ISM in the proxy records potentially implies the presence of a relationship between IO dynamics and the ENSO system. For example, if basin-wide shifts in the IO are influencing shifts in ENSO variance, than

the results here suggest that the IO's direct influence on the monsoon is stronger than from the teleconnections that influence the ISM through ENSO. Additional analyses utilizing long high-resolution proxy reconstructions of IO SSTs (and east–west IO SST gradients) as well as modeling simulations would be needed to constrain whether IO, North Pacific, North Atlantic or additional dynamical mechanisms are driving the coupling between ENSO variance and ISM rainfall in the low-frequency domain.

One possible trajectory towards resolving the mechanism that drives the coupling would be through isolating model simulations that reproduce the observed phase difference between ENSO–ISM coupling in the high- and low-frequency domains. There is some indication in Fig. 6 that realistic phasing between the systems emerges in the GISS model. This is a curious result because this model has a less realistic representation of the ENSO system than the MPI model (Zhang and Jin, 2012). While a larger ensemble of models is certainly needed, the first-pass analysis presented here suggests modeled *coupling* between the ISM and ENSO may be distinct from the robust representation of the two systems independently in the models.

5 Conclusions

Over the last millennium, the ISM has exhibited persistent multidecadal power. The protracted multidecadal shifts in precipitation amounts are significant in considering both flooding and drought frequency in India. The susceptibility of agricultural production to these hydroclimatic changes may increase in coming decades as regional groundwater resources have been severely depleted and therefore may not be able to provide a buffer (Rodell et al., 2009). Through analyses of the phase relationship between proxies for ENSO and the ISM, we show that high-frequency (5–15 yr) shifts in ENSO amplitude yielded a persistent influence on ISM rainfall likely through a previously documented atmospheric teleconnection (Kumar et al., 2006). However, in the low-frequency domain (30–90 yr), periods of increased ENSO variance were coincident with an increase in ISM rainfall. This suggests that the dynamic that couples the systems in the high-frequency domain is not the same as that which couples them in the low-frequency domain. One plausible mechanism to explain this observation is that low-frequency changes in North Atlantic SSTs lead to multidecadal phase locking between ISM rainfall and ENSO variance. This arises due to the presence of an atmospheric teleconnection between the North Atlantic and the ISM and an oceanic teleconnection between the North Atlantic and ENSO variance. Other plausible mechanisms involve low-frequency behavior within the Indian Ocean and North Pacific, which have known influences on the ISM rainfall and may also have a causal link with ENSO. The ENSO system has experienced increased variance during the late 20th century. If the trend in ENSO variance continues, the results presented here do not suggest this will lead to a weakened monsoon. In fact, if the coupling between the systems during the proxy era remained stable, the opposite trend (an increase in ISM rainfall) would be more likely. An assessment of model-simulated ENSO and ISM rainfall under different radiative forcing scenarios would be needed to lend confidence to this assertion, and a methodology to isolate model simulations that correctly capture the coupling between the systems is presented here.

Acknowledgements. We gratefully acknowledge the National Science Foundation grant to A. Sinha (ATM: 0823554) and Chinese National Science Foundation #41230524 and NBRP #2013CB955902 support to H. Cheng for funding a portion of this research.

Edited by: S. Bronnimann

References

Anderson, B. T., Furtado, J. C., Cobb, K. M., and Di Lorenzo, E.: Extratropical forcing of El Niño–Southern Oscillation asymmetry, Geophys. Res. Lett., 40, 4916–4921, doi:10.1002/grl.50951, 2013.

Annamalai, H., Hamilton, K., and Sperber, K.: The South Asian summer monsoon and its relationship with ENSO in the IPCC AR4 simulations, J. Climate, 20, 1071–1092, 2007.

Ashok, K., Guan, Z., Saji, N., and Yamagata, T.: Individual and combined influences of ENSO and the Indian Ocean dipole on the Indian summer monsoon, J. Climate, 17, 3141–3155, 2004.

Berkelhammer, M., Sinha, A., Mudelsee, M., Cheng, H., Edwards, R. L., and Cannariato, K.: Persistent multidecadal power of the Indian Summer Monsoon, Earth Planet. Sc. Lett., 290, 166–172, 2010.

Berkelhammer, M., Sinha, A., Stott, L., Cheng, H., Pausata, F., and Yoshimura, K.: An abrupt shift in the Indian monsoon 4000 years ago, Geoph. Monog. Series, 198, 75–87, 2012.

Buckley, B. M., Anchukaitis, K. J., Penny, D., Fletcher, R., Cook, E. R., Sano, M., Nam, L. C., Wichienkeeo, A., Minh, T. T., and Hong, T. M.: Climate as a contributing factor in the demise of Angkor, Cambodia, P. Natl. Acad. Sci. USA, 107, 6748–52, doi:10.1073/pnas.0910827107, 2010.

Chave, A. D., Thomson, D. J., and Ander, M. E.: On the robust estimation of power spectra, coherences, and transfer functions, J. Geophys. Res., 92, 633–648, doi:10.1029/JB092iB01p00633, 1987.

Cobb, K. M., Charles, C. D., Cheng, H., and Edwards, R. L.: El Niño/Southern Oscillation and tropical Pacific climate during the last millennium, Nature, 424, 271–276, 2003.

Cobb, K. M., Westphal, N., Sayani, H. R., Watson, J. T., Di Lorenzo, E., Cheng, H., Edwards, R., and Charles, C. D.: Highly Variable El Niño–Southern Oscillation Throughout the Holocene, Science, 339, 67–70, 2013.

Collins, M., An, S.-I., Cai, W., Ganachaud, A., Guilyardi, E., Jin, F.-F., Jochum, M., Lengaigne, M., Power, S., Timmermann, A., Vecchi, G., and Wittenberg, A.: The impact of global warming on

the tropical Pacific Ocean and El Niño, Nat. Geosci., 3, 391–397, 2010.

Cook, E. R., Briffa, K. R., Meko, D. M., Graybill, D. A., and Funkhouser, G.: The "segment length curse" in long tree-ring chronology development for palaeoclimatic studies, The Holocene, 5, 229–237, 1995.

Cook, E. R., Woodhouse, C. A., Eakin, C. M., Meko, D. M., and Stahle, D. W.: Long-term aridity changes in the western United States, Science, 306, 1015–1018, 2004.

Cook, E. R., Anchukaitis, K. J., Buckley, B. M., D'Arrigo, R. D., Jacoby, G. C., and Wright, W. E.: Asian monsoon failure and megadrought during the last millennium, Science, 328, 486–489, 2010.

Dansgaard, W.: Stable isotopes in precipitation, Tellus, 16, 436–468, 1964.

D'Arrigo, R., Cook, E. R., Wilson, R. J., Allan, R., and Mann, M. E.: On the variability of ENSO over the past six centuries, Geophys. Res. Lett., 32, L03711, doi:10.1029/2004GL022055, 2005.

Dayem, K. E., Molnar, P., Battisti, D. S., and Roe, G. H.: Lessons learned from oxygen isotopes in modern precipitation applied to interpretation of speleothem records of paleoclimate from eastern Asia, Earth Planet. Sc. Lett., 295, 219–230, 2010.

Dong, B., Sutton, R. T., and Scaife, A. A.: Multidecadal modulation of El Nino–Southern Oscillation (ENSO) variance by Atlantic Ocean sea surface temperatures, Geophys. Res. Lett., 33, L08705, doi:10.1029/2006GL025766, 2006.

Draxler, R. and Rolph, G.: HYSPLIT (HYbrid Single-Particle Lagrangian Integrated Trajectory) model access via NOAA ARL READY website, NOAA Air Resources Laboratory, Silver Spring, available at: http://www.arl.noaa.gov/ready/hysplit4.html last access: March 2012, 2003.

Emile-Geay, J., Cobb, K., Mann, M., and Wittenberg, A.: Estimating Central Equatorial Pacific SST variability over the Past Millennium. Part 2: Reconstructions and Implications, J. Climate, 26, 2329–2352, 2013.

Enfield, D. B., Mestas-Nuñez, A. M., and Trimble, P. J.: The Atlantic Multidecadal Oscillation and its relation to rainfall and river flows in the continental US, Geophys. Res. Lett., 28, 2077–2080, 2001.

Fasullo, J. and Webster, P.: Hydrological signatures relating the Asian summer monsoon and ENSO, J. Climate, 15, 3082–3095, 2002.

Gershunov, A. and Barnett, T.: Interdecadal modulation of ENSO teleconnections, B. Am. Meteorol. Soc., 79, 2715–2725, 1998.

Gershunov, A., Schneider, N., and Barnett, T.: Low-frequency modulation of the ENSO-Indian monsoon rainfall relationship: Signal or noise?, J. Climate, 14, 2486–2492, 2001.

Goswami, B.: Interannual variations of Indian summer monsoon in a GCM: External conditions versus internal feedbacks, J. Climate, 11, 501–522, 1998.

Goswami, B. N., Madhusoodanan, M., Neema, C., and Sengupta, D.: A physical mechanism for North Atlantic SST influence on the Indian summer monsoon, Geophys. Res. Lett., 33, L02706, doi:10.1029/2005GL024803, 2006.

Gupta, A. K., Anderson, D. M., and Overpeck, J. T.: Abrupt changes in the Asian southwest monsoon during the Holocene and their links to the North Atlantic Ocean, Nature, 421, 354–357, 2003.

Huybers, P.: Comments on 'Coupling of the hemispheres in observations and simulations of glacial climate change' by A. Schmittner, O. A. Saenko, and A. J. Weaver, Quaternary Sci. Rev., 23, 207–210, doi:10.1016/j.quascirev.2003.08.001, 2004.

Jourdain, N. C., Gupta, A. S., Taschetto, A. S., Ummenhofer, C. C., Moise, A. F., and Ashok, K.: The Indo-Australian monsoon and its relationship to ENSO and IOD in reanalysis data and the CMIP3/CMIP5 simulations, Clim. Dynam., 41, 3073–3102, 2013.

Krishnamurthy, V. and Goswami, B. N.: Indian monsoon-ENSO relationship on interdecadal timescale, J. Climate, 13, 579–595, 2000.

Krishnan, R. and Sugi, M.: Pacific decadal oscillation and variability of the Indian summer monsoon rainfall, Clim. Dynam., 21, 233–242, 2003.

Kumar, K. K., Rajagopalan, B., and Cane, M. A.: On the weakening relationship between the Indian monsoon and ENSO, Science, 284, 2156–2159, 1999.

Kumar, K. K., Rajagopalan, B., Hoerling, M., Bates, G., and Cane, M.: Unraveling the mystery of Indian monsoon failure during El Niño, Science, 314, 115–119, 2006.

Larkin, N. K. and Harrison, D.: ENSO warm (El Niño) and cold (La Niña) event life cycles: Ocean surface anomaly patterns, their symmetries, asymmetries, and implications, J. Climate, 15, 1118–1140, 2002.

Li, J., Xie, S.-P., Cook, E. R., Huang, G., D'Arrigo, R., Liu, F., Ma, J., and Zheng, X.-T.: Interdecadal modulation of El Niño amplitude during the past millennium, Nature Climate Change, 1, 114–118, 2011.

Mann, M. E., Zhang, Z., Rutherford, S., Bradley, R. S., Hughes, M. K., Shindell, D., Ammann, C., Faluvegi, G., and Ni, F.: Global signatures and dynamical origins of the Little Ice Age and Medieval Climate Anomaly, Science, 326, 1256–1260, 2009.

Mantua, N. and Hare, S.: The Pacific decadal oscillation, J. Oceanogr., 58, 35–44, 2002.

Mudelsee, M.: Climate time series analysis: classical statistical and bootstrap methods, vol. 42, Springer, 2010.

NCDC (NOAA's National Climatic Data Center): "Berkelhammer et al. (2010) – Dandak Cave, India Oxygen Isotope Data" and "Central and Northeast India 1000 Year Stalagmite Oxygen Isotope Data", available at: http://www.ncdc.noaa.gov/paleo/speleothem.html, last access: May 2012,

Pausata, F. S., Battisti, D. S., Nisancioglu, K. H., and Bitz, C. M.: Chinese stalagmite [delta] 18O controlled by changes in the Indian monsoon during a simulated Heinrich event, Nat. Geosci., 4, 474–480, 2011.

Rodell, M., Velicogna, I., and Famiglietti, J. S.: Satellite-based estimates of groundwater depletion in India, Nature, 460, 999–1002, 2009.

Sinha, A., Cannariato, K. G., Stott, L. D., Cheng, H., Edwards, R. L., Yadava, M. G., Ramesh, R., and Singh, I. B.: A 900-year (600 to 1500 AD) record of the Indian summer monsoon precipitation from the core monsoon zone of India, Geophys. Res. Lett., 34, L16707, doi:10.1029/2007GL030431, 2007.

Sinha, A., Berkelhammer, M., Stott, L., Mudelsee, M., Cheng, H., and Biswas, J.: The leading mode of Indian Summer Monsoon precipitation variability during the last millennium, Geophys. Res. Lett., 38, L15703, doi:10.1029/2011GL047713, 2011.

Stahle, D. W., Cleaveland, M., Therrell, M., Gay, D., D'arrigo, R., Krusic, P., Cook, E., Allan, R., Cole, J., Dunbar, R., Moore, M. D., Stokes, M. A., Burns, B. T., Villanueva-Diaz, J., and Thompson, L. G.: Experimental dendroclimatic reconstruction of the Southern Oscillation, B. Am. Meteorol. Soc., 79, 2137–2152, 1998.

Taylor, K. E., Stouffer, R. J., and Meehl, G. A.: An overview of CMIP5 and the experiment design, B. Am. Meteorol. Soc., 93, 485–498, 2012.

Tierney, J. E., Smerdon, J. E., Anchukaitis, K. J., and Seager, R.: Multidecadal variability in East African hydroclimate controlled by the Indian Ocean, Nature, 493, 389–392, 2013.

Timmermann, A., An, S., Krebs, U., and Goosse, H.: ENSO Suppression due to Weakening of the North Atlantic Thermohaline Circulation*, J. Climate, 18, 3122–3139, 2005.

Torrence, C. and Webster, P. J.: Interdecadal changes in the ENSO-monsoon system, J. Climate, 12, 2679–2690, 1999.

Ummenhofer, C. C., Gupta, A. S., Li, Y., Taschetto, A. S., and England, M. H.: Multi-decadal modulation of the El Nino–Indian monsoon relationship by Indian Ocean variability, Environ. Res. Lett., 6, 034006, doi:10.1088/1748-9326/6/3/034006, 2011.

Vuille, M., Werner, M., Bradley, R., and Keimig, F.: Stable isotopes in precipitation in the Asian monsoon region, J. Geophys. Res., 110, D23108, doi:10.1029/2005JD006022, 2005.

Wang, B. and Fan, Z.: Choice of South Asian summer monsoon indices, B. Am. Meteorol. Soc., 80, 629–638, 1999.

Wang, B., Ding, Q., and Joseph, P.: Objective Definition of the Indian Summer Monsoon Onset, J. Climate, 22, 3303–3316, 2009.

Webster, P. J., Maga a, V., Palmer, T., Shukla, J., Tomas, R., Yanai, M., and Yasunari, T.: Monsoons: Processes, predictability, and the prospects for prediction, J. Geophys. Res., 103, 14451–14510, doi:10.1029/97JC02719, 1998.

Yoshimura, K., Kanamitsu, M., Noone, D., and Oki, T.: Historical isotope simulation using reanalysis atmospheric data, J. Geophys. Res., 113, D19108, doi:10.1029/2008JD010074, 2008.

Zhang, W. and Jin, F.: Improvements in the CMIP5 simulations of ENSO-SSTA meridional width, Geophys. Res. Lett., 39, L23704, doi:10.1029/2012GL053588, 2012.